Supporting Information

Mimicking Hydrazine Dehydrogenase for Efficient Electrocatalytic Oxidation of N_2H_4 by Fe-NC

Yan Zheng,[1‡] Fei He,[1‡] Mingxu Chen,[1] Jin Zhang,[2] Guangzhi Hu,[3] Delong Ma,[1] Jinghua Guo,[4] Huailin Fan,[1] Wei Li,[1] and Xun Hu[1*]*

[1] School of Material Science and Engineering, University of Jinan, Jinan 250022, China

[2] Shandong Basan Graphite New Material Plant, Zibo 255300, China

[3] School of Chemical Science and Technology, Yunnan University, Kunming 650504, China

[4] School of Physics and Technology, University of Jinan, Jinan 250022, China

Table of Contents

1. Experimental Section

Materials

Zinc nitrate hexahydrate ($Zn(NO_3)_2$•$6H_2O$, Sinopharm Chemical Reagent Co., Ltd, ⩾ 99.0%), 2-Methylimidazole ($C_4H_6N_2$, Shanghai Macklin Biochemical Co. Ltd, 98%), ethanol (CH_3CH_2OH, Tianjin Fuyu Fine Chemical Co., Ltd, ⩾ 99.7%), methanol (CH_3OH, Tianjin Fuyu Fine Chemical Co., Ltd, ⩾99.5%), iron nitrate ($Fe(NO_3)_3$•$9H_2O$, Aladdin Industrial Corporation).

Preparation of ZIF-8

The synthesis of ZIF-8 was carried out according to the literature with some modifications.[1] In a typical procedure, $Zn(NO_3)_2$•$6H_2O$ (6 mmol) and 2-methylimidazole (MeIM) (24 mmol) were dissolved in 80 mL methanol, respectively. Then the 2-methylimidazole (MeIM) solution was added into the $Zn(NO_3)_2$•$6H_2O$ solution under stirring for 30 min at room temperature. ZIF-8 in the mixed solution was grown under static at room temperature for 24 h. The as-obtained precipitates were centrifuged and washed with ethanol several times and then dried at 60 ^oC for overnight.

Synthesis of Fe-NC

In a typical procedure, the powder of ZIF-8 (500 mg) was dispersed in methanol (10 mL) under ultrasound for 3 min at room temperature. After forming homogeneous dispersed solution, ferric nitrate ($Fe(NO_3)_3$•$9H_2O$) methanol solution (100 mg/mL, 100

μL) was injected into the mixed solution slowly under ultrasound for 2 min at room temperature. Next, the mixed solution was under vigorous stirring for overnight at room temperature in order to make the salt solution be absorbed completely. Then methanol was removed via a rotary evaporator at 35 ^{o}C for 40 min to obtain Fe-doped ZIF-8, which was further placed in a tube furnace and heated to 1000 ^{o}C (heating rate 5 ^{o}C/min) for 2 h in a stream of argon to yield Fe-NC. The calcined products were further immersed with 1 M HCl for 12 h at room temperature and washed with deionized water until the pH was nearly neutral.

The catalyst prepared with different ratio of Fe salt to the mass of ZIF-8 and pyrolyzed at different temperature was denoted as Fe-NC-X-Y (X denoted the mass ratio of Fe salt to ZIF-8, and Y denoted the pyrolyzed temperature. For example, Fe-NC-2-1000 represented the catalyst prepared with the mass ratio of 2% Fe salt to the mass of ZIF-8 and pyrolyzed at 1000 ^{o}C. The content of iron was measured by the inductively coupled plasma mass spectrometry (ICP-MS), the results showed that 0.46 wt%, 0.84 wt% and 1.61 wt% of Fe were found to be present in Fe-NC-1-1000, Fe-NC-2-1000, and Fe-NC-4-1000, respectively.

Synthesis of NC

The powder of ZIF-8 (500 mg) was placed in a tube furnace and heated to 1000 ^{o}C (heating rate 5 ^{o}C/min) for 2 h in a stream of argon to yield NC. The calcined products were further immersed with 1 M HCl for 12 h at room temperature and washed with

deionized water until the pH was nearly neutral. The NC obtained at 1000 °C was denoted as NC-1000.

Electrochemical analysis

Electrocatalytic hydrazine oxidation (HzOR) was performed at room temperature in a three-electrode cell connected to on a CHI760E workstation (CH Instruments, USA). Catalyst-coated glassy carbon electrode (GCE), a graphite rod and a saturated calomel electrode were used as working, counter and reference electrodes, respectively. For the catalyst ink, 4 mg of the catalyst was dispersed in a mixture of 1 mL ethanol and sonicated for 20 min. 20 μL of the ink and 10 μL Nafion (0.05 %) deposited on a 0.19625 cm^2 GCE and dried in air. The mass loading of the synthesized samples on the working electrode was 408 μg/cm^2 and the mass loading of the 20% Pt/C on the working electrode was 100 μg/cm^2. Although the mass loading of Fe-NC-2-1000 was 408 μg/cm^2, the effective Fe content on the working electrode was only 3.43 μg/cm^2 based on the ICP results, which was far lower than that of Pt (20 μg/cm^2). The cyclic voltammetry (CV) was carried out with a potential range from 0 to 1 V (*vs*. RHE) at a scan rate of 10 mV s^{-1} in 1 M KOH solution containing about 100 mM hydrazine. The GCE areas (0.19625 cm^2) were used to calculate the current densities.

The kinetic current was calculated using the following equation:

$$J_K = J_L J / (J_L - J) \qquad \text{Eqn. S1}$$

Where J_k is the kinetic current density, J_L refers to the measured diffusion-limited current density, and J is the experimentally obtained current density.

The values of TOF (e site^{-1} h^{-1}) were calculated using the following equation by assuming that all metal atoms are involved in the catalytic processes:[2]

$$TOF = J \cdot S_{geo} / (F \cdot n) \qquad \text{Eqn. S2}$$

Where J (mA/cm^2) is the as-measured current density at various potential, S_{geo} (0.19625 cm^2) represents the surface area of the glassy carbon disk, F is the Faraday constant (96485 C mol^{-1}), and n is the moles of metal atoms on the electrode, the moles of Fe atoms for Fe-NC-2-1000 can be calculated by the loading weight of catalysts and ICP results. For the NC-1000, the moles of pyridinic N was calculated based on the results of XPS, assuming that the pyridinic N was the active sites according to the reported result.[3]

According to the reported results,[4] ECSA = C/C_s, in which C stands for the measured electrical double layer capacitance, C_s stands for the average double-layer capacitance of 20 μF cm^{-2} for a smooth metal surface according to the reported literature.[4, 5] The *C* was determined by measuring the capacitive current associated with double-layer charging from the scan-rate dependence of cyclic voltammetric stripping. CV curves of the synthesized samples with different scan rates (60, 70, 80, 90, 100 mVs^{-1}) were firstly tested in in 20 mM N_2H_4 (Figure S3a-d). The C was estimated by plotting the $\Delta j / 2 = (j_a - j_c) / 2$ at 0.20 V vs. RHE (where j_c and j_a are the cathodic and

anodic current densities, respectively) against the scan rate, in which the slope was corresponded to C. From the above equation, the ECSA values were derived.

$$E_p = 1/2b \log(\nu) + \text{constant} \quad \text{Eqn. S3}$$

Where E_p refers to the peak potential, b = 2.3RT/[(1−α)n_αF], F is the Faraday constant (96485 C mol^{-1}), the α was calculated based on the linear relationship between the E_p and log(ν) (Figure S3f), the α was 0.5. The value of n_α is estimated to be 1.[6, 7]

Fabrication of N_2H_4-H_2O_2 fuel cell

To assemble the N_2H_4-H_2O_2 fuel cell, the treated Nafion 117 treated with H_2O_2, Fe-NC-2-1000 and 20% Pt/C were used as the electrolyte membrane, anode and cathode catalyst, respectively. The anode was prepared according to the following process: A mixture of carbon black (2 mg) and 5% Nafion (40 mg) was brushed onto a piece of carbon paper (1 cm^2). Then the Fe-NC-2-1000 (4 mg), 5% Nafion (40 mg), 500 μL ethanol and 500 μL deionized water was sonication to form a homogenous dispersion, which was then brushed onto the carbon paper. The loading of Fe-NC-2-1000 catalyst was 4 mg/cm^2, and the cathode was prepared through a similar process, the loading of 20% Pt/C catalyst was 3 mg/cm^2. The N_2H_4-H_2O_2 fuel cell was measured at 80 °C, the cell temperature was controlled by a temperature controller, and its value was monitored by thermocouples. An aqueous solution containing 4 M KOH and 10 wt% N_2H_4 was added into the anode side with a flow rate of 10 mL/min by a silicone tube and a peristaltic pump. Meantime, the liquid fed on the cathode side was an acidic solution,

which contained 20 wt% H_2O_2 and 0.5 M H_2SO_4, with the a flow rate of 14 mL/min by another peristaltic pump. In Such a N_2H_4-H_2O_2 fuel cell, as the electrons transferring from anode to cathode, K^+, as the main charge carrier, could move in an opposite direction through a Nafion membrane.[8] The overall reaction could be written as follows: $N_2H_4 + 2KOH + 2H_2O_2 + H_2SO_4 \rightarrow N_2\uparrow + 6H_2O + K_2SO_4$.

Note: Hydrazine is toxic, flammable and combustible compound. Please use it in the fume hood and store it in a cool and well-ventilated warehouse. It should be noted that using O_2 as cathode is safer compared with H_2O_2, which is worthy of exploring in our future research.

Characterization

X-ray diffraction (XRD, Ultima IV X-ray) with a Cu target (Kα radiation source, λ = 1.5406). The morphologies and energy-dispersive X-ray spectroscopy (EDS) of the samples were observed by high-angle annular dark-field scanning TEM (HAADF-STEM, talos F200X). X-ray photoelectron spectroscopy (XPS) experiments were performed in a Thermo Fisher ESCALAAB 250Xi. Inductively coupled plasma mass spectrometry (ICP-MS) was recorded on an Agilent 7900 instrument (USA). Nitrogen adsorption-desorption isotherms were measured at 77 K with a Quantachrome Autosorb iQ one-station adsorption instrument (USA). Samples were degassed at 300 ^oC for 8 h at redueced pressure before measurement. The surface area was calculated by the Brunauer-Emmett-Teller (BET) method. The surface area and pore volume of

micropores and mesopores was calculated by the V-t method. The pore size distributions (PSD) were calculated based on the model of slit/cylindrical pores on carbon using the dsorption branch of the isotherms by the QSDFT method.

Computational details

The density functional theory (DFT) calculations were performed by using the Vienna Ab Initio Simulation Package (VASP). The exchange-correlation functional is treated using the Perdew Burke Ernzerhof (PBE) generalized-gradient approximation. The cutoff energy for the plane-wave basis set was 500 eV. Structural optimization demonstrates the lattice parameters of a=7.643 Å and b=7.589 Å. The Brillouin zone was sampled by 7 × 7 × 1 k-points. Between the two consecutive steps, the convergence criterion for the self-consistent calculation of ion relaxation was set as 10^{-5} eV. All cell sizes and atom positions was optimized by using the conjugate gradient method until the atomic force is less than 0.02 eVÅ^{-1}.

2. Supplementary Figures and Tables

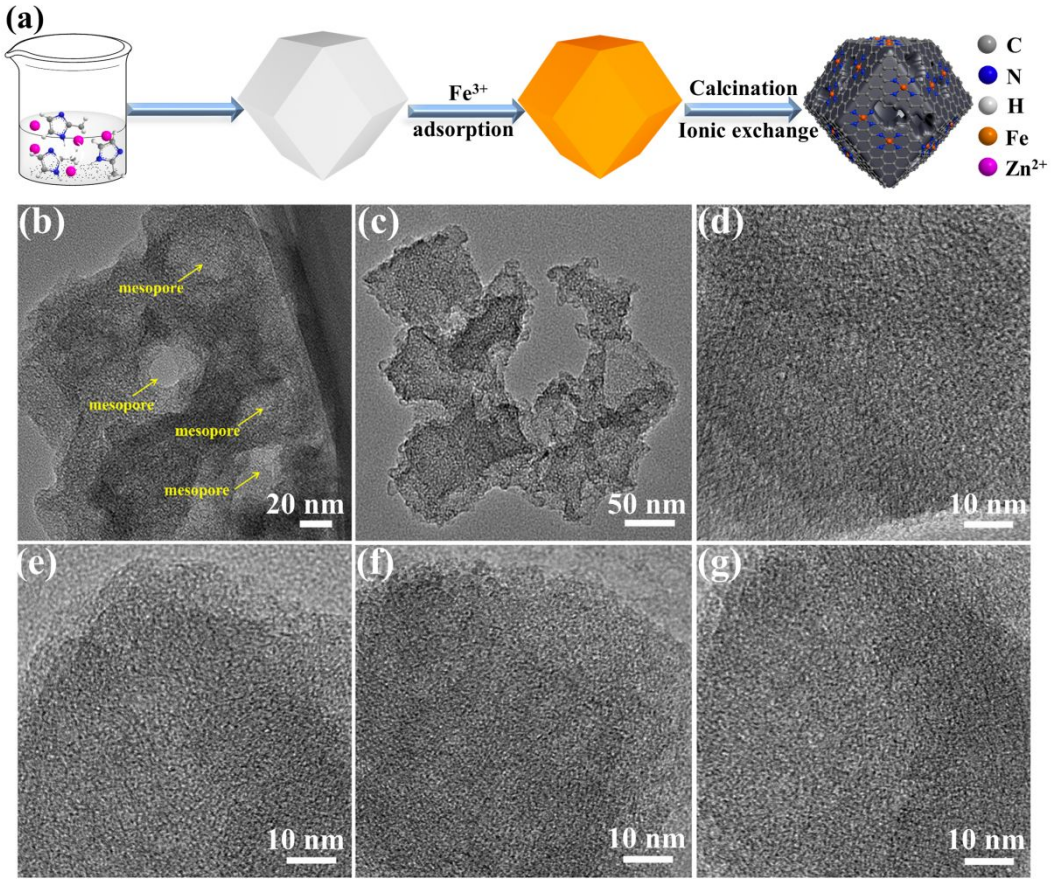

Figure S1. (a) Schematic illustration of the synthesis process of Fe-NC. (b) HRTEM images of Fe-NC-2-1000. (c) HRTEM images of NC-1000. (d-g) HRTEM images of Fe-NC-2-1000 with different areas.

Table S1. The percentage of C and N for samples based on the XPS results.

Sample	C / at.%	N / at.%
NC-1000	92.03	7.97
Fe-NC-1-1000	91.76	5.06
Fe-NC-2-1000	89.55	6.62
Fe-NC-4-1000	92.44	4.76

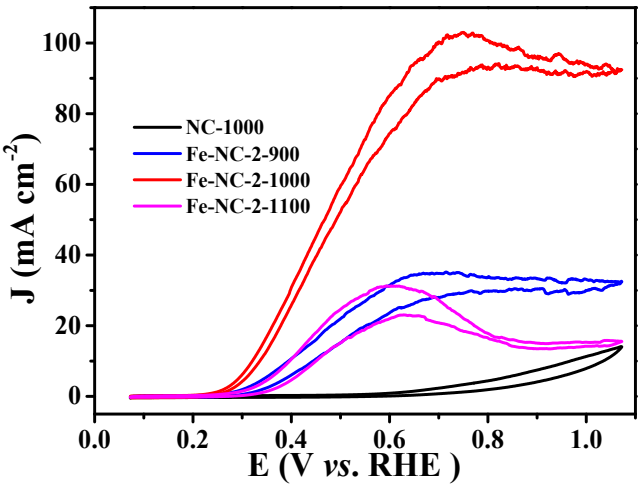

Figure S2. The CVs of Fe-NC-2-1000 prepared at different temperature (100 mM N_2H_4, 1 M KOH, scan rate 10 mV/s).

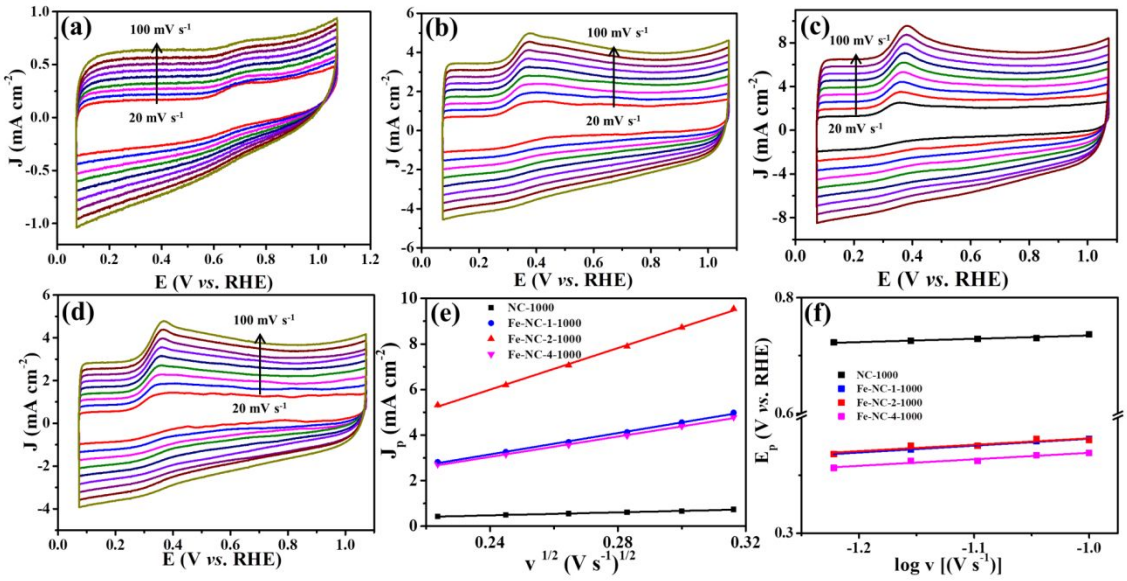

Figure S3. CV tests at different scan rates: (a) NC-1000; (b) Fe-NC-1-1000; (c) Fe-NC-2-1000; (d) Fe-NC-4-1000. (e) The linear dependence of peak current density (J_p) of HzOR over catalysts in relation to the square root of scan rate ($v^{1/2}$). (f) Plot of peak potential (E_p) vs. log of scan rate (log υ) obtained from the same conditions. Experiment condition: 1 M KOH containing about 20 mM hydrazine.

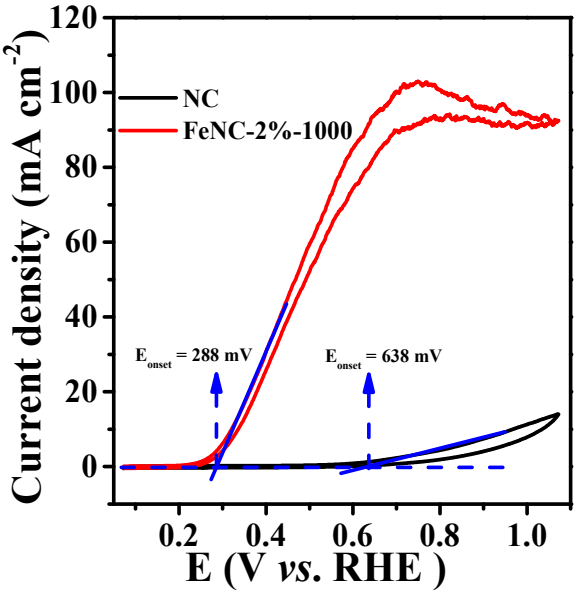

Figure S4. The onset potential for NC-1000 and Fe-NC-2-1000.

Table S2. Comparison of electrocatalytic HzOR activity of the reported other metal-containing and metal-free doped carbon catalysts.

	Catalysts	Electrolyte	N_2H_4 (mM)	E_{onset} V vs.RHE	E_{peak} V vs. RHE	J_{peak} (mA cm^{-2})	References
1	Fe-NC-2-1000	1 M KOH	100	0.28	0.75	103.03	This work
2	NSC	0.1 M PBS	50	0.43	0.68	2.92	6
3	Cu–GP	0.1 M KOH	10	1.04	1.31	1.56	7
4	wash-Fe_2MoC@NC	1 M KOH	100	0.28	0.58	12.77	9
5	SeNCM	1 M KOH	100	0.34	0.78	30.8	10
6	PolyCuDAB–CB	0.1 M KOH	10	0.61	0.79	11.60	11
7	Cu NCs / AC	0.1 M KOH	100	0.60	1.38	20.00	12
8	Vap-PM-CNF	1 M KOH	100	0.36	0.65	10	13
9	flower-shaped CuO	0.1 M KOH	100	1.01	1.27	4.89	14
10	MnO/N-C	1 M KOH	100	0.40	1.10	6.28	15
11	CuO/C	0.1 M KOH	10	0.98	1.30	4.59	16
12	Fe_2O_3/ECP-15	1 M KOH	100	0.67	0.89	89.57	17
13	PNC3	0.01 M PBS	100	0.42	0.70	4.37	18
14	h-$MnFe_2O_4$NPs/N-rGO	0.1 M PBS	1	0.43	0.73	0.75	19
15	CaSC-Co^R	0.1 M PBS	50	0.34	0.51	2.02	20
16	CaSC-Co	0.1 M PBS	50	0.37	0.56	2.21	20
17	CaSC-Fe	0.1 M PBS	50	0.44	0.66	1.70	20
18	CaSC-Fe^R	0.1 M PBS	50	0.28	0.59	1.80	20
19	S-RGO/Cu	0.1 M KOH	10	0.98	1.28	14.68	21
20	Cu	1 M KOH	400	0.32	0.57	43.07	22
21	PPY-NOMPCs	0.1 M PBS	100	0.41	0.64	4.30	23
22	PCDF-900	0.1 M PBS	50	0.43	0.72	2.53	24

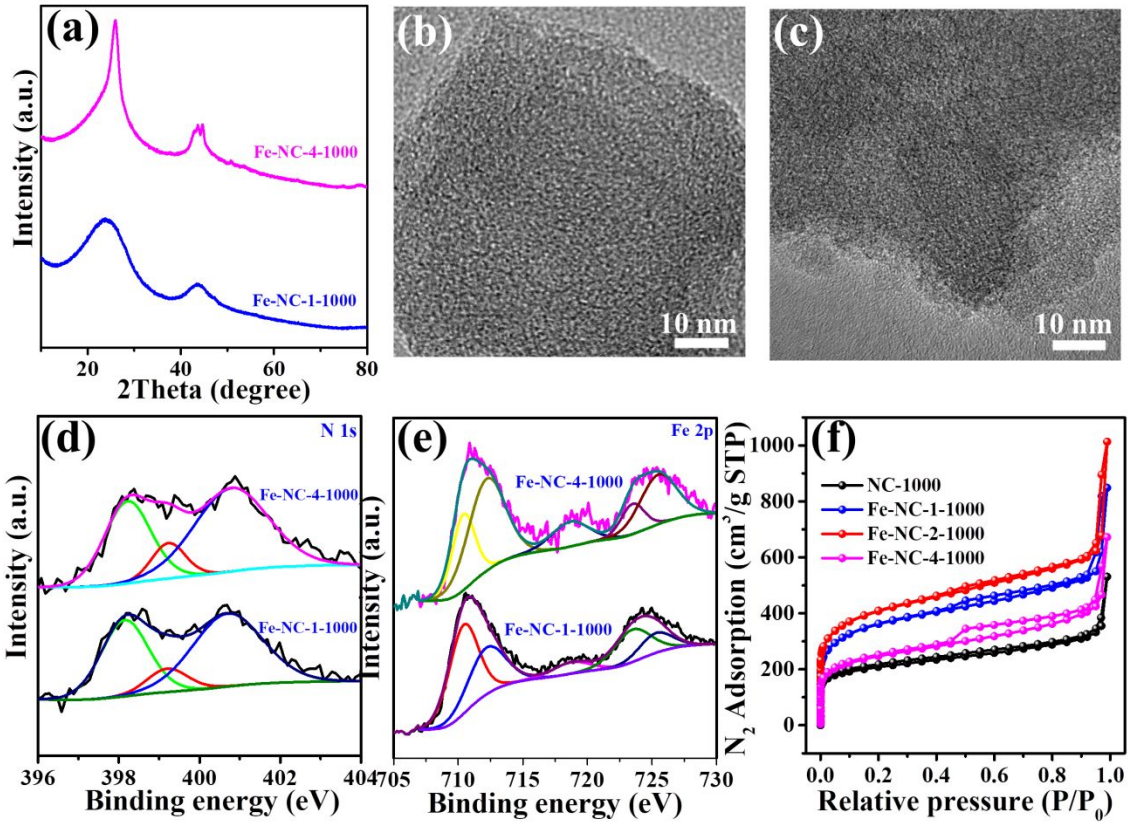

Figure S5. (a) XRD patterns of NC-1000 and Fe-NC-2-1000. (b) HRTEM images of Fe-NC-1-1000. (c) HRTEM images of Fe-NC-4-1000. (d) XPS spectra of Fe-NC-1-1000 and Fe-NC-4-1000 in the regions of N 1s. (e) XPS spectra of Fe-NC-1-1000 and Fe-NC-4-1000 in the regions of Fe 2p. (f) N_2 adsorption–desorption isotherms of NC-1000, Fe-NC-1-1000, Fe-NC-2-1000 and Fe-NC-4-1000.

Compared with NC-1000, the XRD pattern of Fe-NC-2-1000 (Figure 2c) showed a poorer (002) peak intensity. In addition, based on the controlled experiments (Figure 2c and Figure S5a), it was found that Fe-NC-1-1000 and Fe-NC-2-1000 showed the similar (002) peak intensity due to their low content of Fe. However, when the content of Fe in the precursor further increased, an enhanced (002) peak was obviously for the formed

catalyst (Fe-NC-4-1000) (Figure S5a). Such a result further demonstrated that the low content of Fe hardly enhanced graphitization effectively.[25]

Table S3. The [a]ECSA of samples.

Sample	ECSA (m^2/g)
NC-1000	86
Fe-NC-1-1000	453
Fe-NC-2-1000	380
Fe-NC-4-1000	846

[a]The ECSA of samples was calculated based on the reference 4 and 5 in the SI.

The ECSA was calculated to be 86, 453, 846 and 380 m^2/g for NC-1000, Fe-NC-1-1000, Fe-NC-2-1000 and Fe-NC-4-1000, respectively.

Table S4. Mesopore surface area (MSA) and mesopore volume (MV) of NC-1000, Fe-NC-1-1000, Fe-NC-2-1000 and Fe-NC-4-1000

Samples	mesopore surface area (m^2/g)	mesopore volume (cc/g)
NC-1000	288	0.32
Fe-NC-1-1000	577	0.59
Fe-NC-2-1000	631	0.62
Fe-NC-4-1000	598	0.56

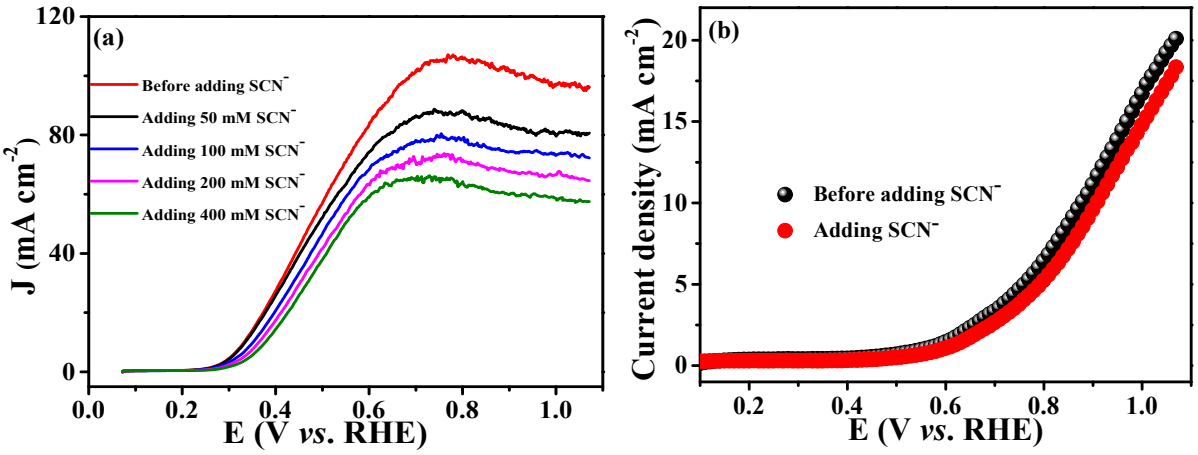

Figure S6. (a) LSV curves of Fe-NC-2-1000 and the response of Fe-NC-2-1000 to different concentration of SCN^- poisoning in 1 M KOH. (b) LSV curves of NC-1000 and the response of NC-1000 to SCN^- poisoning in 1 M KOH.

As a poisoning reagent, SCN^- was able to complex with Fe to block the Fe-N centers.[26, 27] However, in 1 M KOH solution, the OH^- had been also demonstrated to a ligand, which could coordinate with Fe.[26] Thus, during electrocatalytic HzOR (N_2H_4 + $4OH^- \rightarrow N_2 + 4H_2O$), there was competitive effect between SCN^- and OH^-. Although the content of SCN^- (5 mmol or 50mM) far exceeded the amount of Fe sites (~0.06 □mol), the Fe-N centers hardly poisoned completely in 1 M KOH solution (Figure 2d). Rinsing the SCN^--poisoned Fe-NC-2-1000 electrode with water could largely recover the HzOR activity (Figure 2d). Moreover, it was found that even if the SCN^- content increased to 400 mM, the Fe-NC-2-1000 still kept the electrocatalytic HzOR activity. Therefore, when

adding more SCN^- to the 1 M KOH, the HzOR activity of Fe-NC-2-1000 would become poorer, but hardly lost activity completely, due to the existence of a competitive effect between SCN^- and OH^-.

Supplementary References

(1) Zhao, C.; Dai, X.; Yao, T.; Chen, W.; Wang, X.; Wang, J.; Yang, J.; Wei, S.; Wu, Y.; Li, Y., Ionic Exchange of Metal-Organic Frameworks to Access Single Nickel Sites for Efficient Electroreduction of CO_2. *J. Am. Chem. Soc*. **2017**, *139*, 8078-8081.

(2) Xie, J.; Zhang, X.; Zhang, H.; Zhang, J.; Li, S.; Wang, R.; Pan, B.; Xie, Y., Intralayered Ostwald Ripening to Ultrathin Nanomesh Catalyst with Robust Oxygen-Evolving Performance. *Adv. Mater.* **2017**, *29*, 1604765-1604772.

(3) Zhang, T.; Asefa, T., Heteroatom-Doped Carbon Materials for Hydrazine Oxidation. *Adv. Mater.* **2019**, *31*, 1804394-1804401.

(4) Li, Q.; Wu, G.; Cullen, D. A.; More, K. L.; Mack, N. H.; Chung, H. T.; Zelenay, P., Phosphate-Tolerant Oxygen Reduction Catalysts. *ACS Catal.* **2014**, *4*, 3193-3200.

(5) Gao, S.; Lin, Y.; Jiao, X.; Sun, Y.; Luo, Q.; Zhang, W.; Li, D.; Yang, J.; Xie, Y., Partially oxidized atomic cobalt layers for carbon dioxide electroreduction to liquid fuel. *Nature* **2016**, *529*, 68-71.

(6) Cazetta, A. L.; Zhang, T.; Silva, T. L.; Almeida, V. C.; Asefa, T., Bone char-derived metal-free N- and S-co-doped nanoporous carbon and its efficient electrocatalytic activity for hydrazine oxidation. *Appl. Catal., B* **2018**, *225*, 30-39.

(7) Gao, H.; Wang, Y.; Xiao, F.; Ching, C. B.; Duan, H., Growth of Copper Nanocubes on Graphene Paper as Free-Standing Electrodes for Direct Hydrazine Fuel Cells. *J. Phys. Chem. C* **2012**, *116*, 7719-7725.

(8) Feng, G.; Kuang, Y.; Li, P.; Han, N.; Sun, M.; Zhang, G.; Sun, X., Single Crystalline Ultrathin Nickel-Cobalt Alloy Nanosheets Array for Direct Hydrazine Fuel Cells. *Adv. Sci.* **2017**, *4*, 1600179-1600179.

(9) Ojha, K.; Farber, E. M.; Burshtein, T. Y.; Eisenberg, D., A Multi‐Doped Electrocatalyst for Efficient Hydrazine Oxidation. *Angew. Chem. Int. Ed.* **2018**, *57*, 17168-17172.

(10) Wang, T.; Wang, Q.; Wang, Y.; Da, Y.; Zhou, W.; Shao, Y.; Li, D.; Zhan, S.; Yuan, J.; Wang, H., Atomically Dispersed Semimetallic Selenium on Porous Carbon Membrane as an Electrode for Hydrazine Fuel Cells. *Angew. Chem.* **2019**, *131*, 13600-13605.

(11) He, F.; Mi, L.; Shen, Y.; Chen, X.; Yang, Y.; Mei, H.; Liu, S.; Mori, T.; Zhang, Y., Driving electrochemical oxygen reduction and hydrazine oxidation reaction by enzyme-

inspired polymeric Cu(3,3′-diaminobenzidine) catalyst. *J. Mater. Chem. A* **2017**, *5*, 17413-17420.

(12) Gao, X.; Du, C.; Zhang, C.; Chen, W., Copper Nanoclusters on Carbon Supports for the Electrochemical Oxidation and Detection of Hydrazine. *ChemElectroChem* **2016**, *3*, 1266-1272.

(13) Jeong, J.; Choun, M.; Lee, J., Tree-Bark-Shaped N-Doped Porous Carbon Anode for Hydrazine Fuel Cells. *Angew Chem Int Ed* **2017**, *56*, 13513-13516.

(14) Ma, Y.; Wang, H.; Key, J.; Ji, S.; Lv, W.; Wang, R., Control of CuO nanocrystal morphology from ultrathin “willow-leaf” to “flower-shaped” for increased hydrazine oxidation activity. *J. Power Sources* **2015**, *300*, 344-350.

(15) Ding, J.; Kannan, P.; Wang, P.; Ji, S.; Wang, H.; Liu, Q.; Gai, H.; Liu, F.; Wang, R., Synthesis of nitrogen-doped MnO/carbon network as an advanced catalyst for direct hydrazine fuel cells. *J. Power Sources* **2019**, *413*, 209-215.

(16) Ma, Y.; Li, H.; Wang, R.; Wang, H.; Lv, W.; Ji, S., Ultrathin willow-like CuO nanoflakes as an efficient catalyst for electro-oxidation of hydrazine. *J. Power Sources* **2015**, *289*, 22-25.

(17) Wang, Y.; Chen, Z.; Wu, H.; Xiao, F.; Cao, E.; Du, S.; Wu, Y.; Ren, Z., Self-Assembly-Induced Mosslike Fe_2O_3 and FeP on Electro-oxidized Carbon Paper for Low-Voltage-Driven Hydrogen Production Plus Hydrazine Degradation. *ACS Sustainable Chem. Eng.* **2018**, *6*, 15727-15736.

(18) Silva, T. L.; Cazetta, A. L.; Zhang, T.; Koh, K.; Silva, R.; Asefa, T.; Almeida, V. C., Nanoporous Heteroatom-Doped Carbons Derived from Cotton Waste: Efficient Hydrazine Oxidation Electrocatalysts. *ACS Appl. Energy Mater.* **2019**, *2*, 2313-2323.

(19) Khilari, S.; Pradhan, D., $MnFe_2O_4$@nitrogen-doped reduced graphene oxide nanohybrid: an efficient bifunctional electrocatalyst for anodic hydrazine oxidation and cathodic oxygen reduction. *Catal. Sci. Technol.* **2017**, *7*, 5920-5931.

(20) Fragal, V. H.; Fragal, E. H.; Zhang, T.; Huang, X.; Cellet, T. S. P.; Pereira, G. M.; Jitianu, A.; Rubira, A. F.; Silva, R.; Asefa, T., Deriving Efficient Porous Heteroatom-Doped Carbon Electrocatalysts for Hydrazine Oxidation from Transition Metal Ions-Coordinated Casein. *Adv. Funct. Mater.* **2019**, *29*, 1808486-1808497.

(21) Liu, C.; Zhang, H.; Tang, Y.; Luo, S., Controllable growth of graphene/Cu composite and its nanoarchitecture-dependent electrocatalytic activity to hydrazine oxidation. *J. Mater. Chem. A* **2014**, *2*, 4580-4587.

(22) Granot, E.; Filanovsky, B.; Presman, I.; Kuras, I.; Patolsky, F., Hydrazine/air direct-liquid fuel cell based on nanostructured copper anodes. *J. Power Sources* **2012**, *204*, 116-121.

(23) Meng, Y.; Zou, X.; Huang, X.; Goswami, A.; Liu, Z.; Asefa, T., Polypyrrole-derived nitrogen and oxygen co-doped mesoporous carbons as efficient metal-free electrocatalyst for hydrazine oxidation. *Adv. Mater.* **2014**, *26*, 6510-6516.

(24) Martins, A. C.; Huang, X.; Goswami, A.; Koh, K.; Meng, Y.; Almeida, V. C.; Asefa, T., Fibrous porous carbon electrocatalysts for hydrazine oxidation by using cellulose filter paper as precursor and self-template. *Carbon* **2016**, *102*, 97-105.

(25) Zhang, H.; Hwang, S.; Wang, M.; Feng, Z.; Karakalos, S.; Luo, L.; Qiao, Z.; Xie, X.; Wang, C.; Su, D., Single Atomic Iron Catalysts for Oxygen Reduction in Acidic Media: Particle Size Control and Thermal Activation. *J. Am. Chem. Soc.* **2017**, *139*, 14143-14149.

(26) Yang, X.; Xia, D.; Kang, Y.; Du, H.; Kang, F.; Gan, L.; Li, J., Unveiling the Axial Hydroxyl Ligand on Fe-N_4-C Electrocatalysts and Its Impact on the pH‐Dependent Oxygen Reduction Activities and Poisoning Kinetics. *Adv. Sci.* **2020**, 2000176-2000182.

(27) Jiang, W.-J.; Gu, L.; Li, L.; Zhang, Y.; Zhang, X.; Zhang, L.-J.; Wang, J.-Q.; Hu, J.-S.; Wei, Z.; Wan, L.-J., Understanding the high activity of Fe–N–C electrocatalysts in oxygen reduction: Fe/Fe_3C nanoparticles boost the activity of Fe–N x. *J. Am. Chem. Soc.* **2016**, *138*, 3570-3578.